Geophysical Journal International

Geophys. J. Int. (2010) doi: 10.1111/j.1365-246X.2010.04488.x

Core structure re-examined using new teleseismic data recorded in Antarctica: evidence for, at most, weak cylindrical seismic anisotropy in the inner core

Daniel Leykam,[1] Hrvoje Tkalčić[1] and Anya M. Reading[2]

[1] *Research School of Earth Sciences, The Australian National University, Mills Road, Canberra* 0200 ACT, *Australia. E-mail: Hrvoje.Tkalcic@anu.edu.au*
[2] *School of Earth Sciences, University of Tasmania, Private Bag* 79, TAS 7001, *Australia*

Accepted 2009 December 16. Received 2009 November 4; in original form 2009 July 2

SUMMARY

We present a significant addition to the data set of traveltimes of seismic PKP waves that sample the Earth's lowermost mantle and core along the Earth's rotation axis. Recorded at permanent Global Seismic Network (GSN) and temporary SSCUA deployment broadband seismographic stations in Antarctica, the new data improve the previously poor and biased coverage that underlies the seismic constraints on recent models of inner core structure and anisotropy. On the one hand, new differential PKP traveltime measurements improve the sampling of predominantly the eastern inner core hemisphere. PKPab-df and PKPbc-df differential traveltime residuals, with respect to the spherically symmetric model ak135, are consistently smaller than two seconds along the north–south paths sampled. Axially symmetric models of inner core seismic anisotropy with fast axis parallel to the Earth's rotation axis require a weak anisotropy of (0.7 ± 0.1) per cent to be consistent with our PKPbc-df observations. PKPbc-df residuals from the quasi-eastern hemisphere indicate (0.4 ± 0.1) per cent anisotropy. If only PKPbc-df observations from the top 200 km of this hemisphere are considered, this is reduced to (0.1 ± 0.2) per cent, consistent with an isotropic layer. On the other hand, new absolute PKP traveltime measurements add to the sampling of both hemispheres of the inner core, but it is difficult to use them with more confidence to assess structure of the core since they are affected by crustal and mantle structure and source uncertainties. The newly collected data set also increases constraints on D" structure beneath the South Pole. In contrast to previous inferences based on data from northern stations, we find no evidence of a velocity heterogeneity in the outer core near the inner core boundary associated with the cylinder tangent to the inner core in the southern hemisphere.

Key words: Composition of the core; Body waves; Seismic anisotropy; Antarctica.

1 INTRODUCTION

The Earth's core is routinely studied with normal modes (free oscillations of the Earth sensitive to the entire volume of the Earth) (e.g. Dziewonski & Anderson 1981) and body waves, such as PKP waves (i.e. compressional waves that traverse the Earth's core). The focus of this paper is on PKP waves observed in Antarctica, whose traveltimes were analysed and interpreted in the context of the existing hypotheses of the core structure. Inner core structure may be inferred through direct observation of the traveltimes of PKIKP (PKPdf branch) waves travelling through it (absolute traveltimes), or by relative analysis of traveltimes of PKIKP and other PKP phases that bottom in the outer core, such as PKPbc and PKPab (differential traveltimes). For the illustration of the ray-paths of PKP waves, see Fig. 1.

1.1 Lack of spatial coverage of the inner core by PKP waves

The inner core is well sampled along equatorial paths with PKP waves (i.e. compressional waves that traverse the inner core semi-parallel to the Earth's equator) due to the large number of favourable source–receiver configurations. The coverage of the inner core along polar paths with PKP waves is relatively sparse due to the lack of large earthquakes and seismic stations at suitable locations. As inner core sensitive phases such as PKIKP (PKPdf) are only observed at large epicentral distances, sampling along polar paths requires both the large size earthquake and the receiving station to be located at extreme geographic latitudes. The South Sandwich Islands (SSI) to Alaska path provides the most anomalous traveltime data and forms the basis for several inner core anisotropy models,

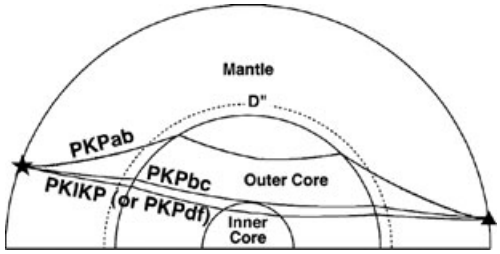

Figure 1. Cross-section of Earth showing three main phases of PKP waves traversing the core.

including the finding that the quasi-western hemisphere of the inner core is anisotropic and significantly different from the quasi-eastern hemisphere (see next section or Tkalčić & Kennett (2008) for references). It is difficult to place close constraints on these models with such limited coverage. There are a few other locations in the southern oceans, such as Bouvet Island in the South Atlantic, Southeast Indian Ridge and Western Indian–Antarctic Ridge in the South Indian Ocean, and the Macquarie Islands region in the south west corner of the Pacific Ocean that produce earthquakes large enough to generate detectable PKP waves in the north, but they are sparse. On the other hand, earthquakes distributed along the northern part of the Pacific Rim, such as those in the Aleutian Islands area and Alaska, as well as those that stretch between Iceland and the Svalbard archipelago in the Arctic Ocean present a great potential for the observations of PKP waves in Antarctica.

1.2 Inner core anisotropy

Poupinet *et al*. (1983) found that PKP waves passing through the inner core travelled faster in the direction semi-parallel to the Earth's rotation axis and arrived earlier than predicted by reference earth models. To explain these anomalous traveltimes, an anisotropic structure of the inner core was hypothesized by Morelli *et al*. (1986) and Woodhouse *et al*. (1986). For PKP waves traversing the core, a fast axis of anisotropy is hypothesized in the same direction as the wave propagation.

Iron crystals in the inner core may align to form an anisotropic medium, but the mechanism remains under debate. Alignment during solidification may be caused by a strong toroidal field (Karato 1993), the formation of a single crystal (Stixrude & Cohen 1995), or solidification texturing (Bergman 1997). Proposed mechanisms for later alignment include inner core convection (Jeanloz & Wenk 1988), strain resulting from solidification rates varying with latitude (Yoshida *et al.* 1996) or Maxwell stresses (Karato 1999; Buffet & Wenk 2001). Low bounds on meridional anisotropy are inconsistent with inner core convection or magnetic stresses being significant causes (Helffrich *et al.* 2002). Experiments (Bergman *et al.* 2005) indicate that the inner core may solidify faster near the equator, which would favour cylindrical symmetry if deformations after solidification are insignificant.

Several hypotheses of inner core anisotropy have been proposed. Early studies suggested constant anisotropy of up to 3.5 per cent throughout the inner core (Creager 1992). Tanaka & Hamaguchi (1997) showed that anisotropy may only be present in the quasi-western hemisphere of the inner core. Tkalčić *et al.* (2002) confirmed a hemispheric dependence of seismic properties (PKP differential traveltimes) using carefully assembled global data set of PKP differential traveltimes. Their Figs 3 and 4 illustrate differential traveltime residuals as a function of angle of sampling the inner core, where data are placed in the geographical context. Their data set included a number of measurements made on seismograms recorded at SPA and SYO stations and a small number of measurements at SNA and SBA, all prior to year 2000. A significant scatter of PKPab-df traveltime residuals observed at SPA was evident, while PKPab-df data from SYO showed predominantly small traveltime residuals. There was a much less scatter evident in PKPbc-df data, with most Antarctic data falling within a range that is not considered anomalous. This was clearly not the case for the data from the South Atlantic Ocean earthquakes observed in the north. There were other studies that also confirmed the existence of the hemispherical pattern in PKP differential traveltimes. For example, Wen & Niu (2002) used 26 PKPbc observations from the Antarctic stations SPA and SYO to confirm the hemispherical pattern of inner core anisotropy. Some studies have found that the inner core may be isotropic near the inner core boundary (e.g. Song & Helmberger 1998; Ouzounis & Creager 2001). An asymmetric model was developed (e.g. Creager 1999; Garcia 2001) to fit these new observations. An innermost inner core (IMIC) with different anisotropic properties has also been hypothesized by Ishii & Dziewonski (2002). Cormier & Stroujkova (2005) determined through the modelling of waveforms that either the IMIC had a radius greater than 450 km or its boundary was not discrete. Calvet *et al.* (2006) found that three different models of IMIC anisotropy were capable of explaining the observations and noted that more data from high latitude stations were required to more closely constrain its structure. Garcia *et al*. (2006) have also not found evidence for the innermost inner core from a new data set of PKP waves. For a more detailed description of inner core anisotropy, see a review by Tkalčić & Kennett (2008).

1.3 Lowermost mantle and the outer core

The major difficulty in studying the inner core is isolating the effects of the inner core from heterogeneity in the mantle, particularly at the core–mantle boundary (CMB). Although the use of differential traveltimes tends to reduce errors due to mantle structure, it is not without problems. PKPdf diverges from PKPbc and PKPab in the lowermost mantle and may be influenced by short, medium and long scale structures (e.g. Doornbos 1974; Haddon & Cleary 1974; Snoke & Sacks 1986; Wysession *et al*. 1992; Helffrich & Sacks 1994; Souriau & Poupinet 1994; Garnero & Helmberger 1995; Sylvander *et al.* 1997; Bréger *et al.* 1999, 2000; Thomas *et al.* 2002; Tkalčić *et al.* 2002; Restivo & Helffrich 2006). Tkalčić *et al.* (2002) showed that structure at the bottom of the mantle could explain a significant amount of PKPab-df observations. They proposed this as an alternative to complexity in the inner core, although mantle structure could not completely explain their PKPbc-df data set. Small scale heterogeneity in the lowermost mantle, either alone or combined with inner core anisotropy, could explain the observations, but such a model is not yet well constrained. They demonstrated that the South Sandwich Islands to Alaska anomalous data are difficult to explain, even when the mantle heterogeneity and core anisotropy contributions are combined. Ishii *et al.* (2002a,b) also argued that differential traveltime data may be contaminated by biased sampling of particular paths. Their simple model of constant inner core anisotropy provided a good fit to normal mode and PKPdf data.

Models involving simple inner core structure combined with heterogeneity in the outer core, in a cylinder tangent to the inner core, have also been proposed to explain the observed normal modes (Romanowicz & Bréger 2000) and body wave data (Romanowicz *et al.* 2003). Romanowicz *et al.* (2003) modelled a region of

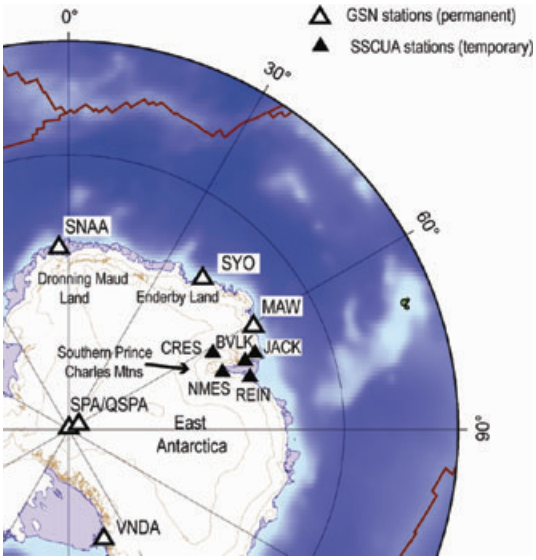

Figure 2. Locations of the receiving stations.

1 per cent faster *P* velocity within this cylinder and found that it could reproduce the characteristic L-shape pattern of observed residuals along quasi-polar paths (e.g. for the differential traveltime residuals as a function of the angle between PKPdf in the inner core and the rotation axis of the Earth, see Fig. 5). That study consisted of mostly of PKP data from South Atlantic recorded in Alaska, therefore sampling the northern part of the tangent cylinder. Recent studies, however, have argued that there is no significant velocity anomaly within the tangent cylinder (e.g. Souriau *et al.* 2003; Ishii & Dziewonski 2005; Yu *et al.* 2005).

In this paper, we present a new data set of PKP traveltime measurements recorded at stations on the Antarctic continent, which significantly improves the sampling of the core along polar paths. This study is focused on the inner-core sensitive events, occurring between 2001 and 2006, and recorded at selected permanent seismic stations in East Antarctica and at the South Pole, and some of the temporary stations of the SSCUA deployment (Reading 2006). With this complementary data set, we are thus able to re-examine recent models of inner core structure and anisotropy using more widely sampled seismic constraints.

2 DATA SETS AND DATA SELECTION

The events were observed at the GSN stations SNAA, QSPA, SPA, SYO, MAW, VNDA and CASY and the stations BVLK, JACK, CRES, NMES and REIN from the SSCUA deployment (Reading 2006; Fig. 2; see tables in the Appendix). Only 14 of our new PKPbc-df measurements are from stations SPA and SYO, whose data prior to 2002 were analysed in earlier studies (Niu & Wen 2002; Tkalčić *et al.* 2002), as mentioned in Section 1.2. Our SYO and SPA subset, however, is complementary to that published earlier, as it considers earthquakes from 2002 to the present day. The rest of our data are from SNAA (the majority), SSCUA, and a small number from the other GSN stations. The SSCUA stations were remote, solar powered station sets deployed using helicopter and fixed-wing air support by small field parties. The stations were shut down automatically during the dark winter months and were revisited the following summer to download recorded data. Events before 2006 were relocated using the catalogue of Engdahl *et al.* (1998). Most measurements originate from shallow and intermediate depth earthquakes between Japan and Alaska.

The new data set consists of manually picked traveltimes of PKPdf, PKP(ab-df) and PKP(bc-df) seismic phases from Antarctic stations from 2001 to 2006. A total of 83 PKPdf (12 from SSCUA), 49 PKPbc-df (8 from SSCUA) and 26 PKPab-df (3 from SSCUA) measurements were taken. Recordings from the Antarctic stations typically had a poor signal-to-noise ratio, except for a few large magnitude events. For example, the SSCUA stations had a relatively poor signal-to-noise ratio owing to their locations near ice streams associated with the Lambert Glacier. The attenuation of PKPdf in the inner core and high magnitude, low frequency noise tended to hide the arrival of PKPdf. Whenever possible, PKP arrival times were picked without filtering. For events with a lower signal-to-noise ratio, a five pole causal high pass filter with corner frequency 1.0 Hz was applied. Seismograms with a poor signal-to-noise ratio or an unclear PKPdf arrival were discarded. The station SNAA consistently recorded the best signals and provided most of the new measurements (42 PKPdf, 25 PKPbc-df, 21 PKPab-df). QSPA also provided high quality measurements, but it was not operational for the whole time period.

For the differential traveltime measurements, an acausal five pole bandpass filter between 0.5 and 2.0Hz was applied. Then the PKPbc and Hilbert transformed PKPab phases were superimposed over the reference PKPdf arrival. The time-shift required for the best match with the reference phase was recorded as the differential traveltime. It was necessary to scale the waveforms to assist the comparison, as the amplitude of PKPdf was significantly lower than PKPbc and PKPab. Due to inner core attenuation of high frequencies, the PKPdf waveform is typically broader than PKPab and PKPbc. Priority was given to matching the first peaks, where the phase difference was minimal.

Some examples of the measurement technique are displayed below in Fig. 3. Approximately one-third of the measurements were of a similar quality, while the rest were noisier. After a visual inspection of 97 seismograms, quality A was assigned to the best measurements, B to the acceptable and C to the questionable data. Measurements of quality C were not used. The PKPdf data have a scatter of approximately 4 s, as expected due to errors in epicentral location and mantle heterogeneity. PKPab-df and PKPbc-df have smaller spreads of 3 and 2 s, respectively.

All residuals were calculated with respect to the model ak135 (Kennett *et al.* 1995) and were corrected for ellipticity. Corrections for mantle structure could not be made because there were insufficient data for previous studies to adequately model D" structure beneath polar regions (Tkalčić *et al.* 2002), which might influence absolute and differential time measurements significantly. Smoother tomography maps that are available will have a similar impact on traveltimes.

The new data set is small compared to previous studies, such as the 420 PKPdf, 922 PKPbc-df and 1453 PKPab-df measurements assembled in Tkalčić *et al.* (2002) or even larger (although lower in quality) data set assembled in Garcia *et al.* (2006). However, the new measurements sample paths poorly covered in the previous data sets. Most of the polar path measurements in Tkalčić *et al.* (2002) were made at Alaskan and Siberian stations, with several exceptions measured mostly on SPA and SYO stations in Antarctica, while the new data set focuses specifically on north–south paths observed in Antarctica. This improved coverage is required to identify any bias present in the paths responsible for most polar measurements.

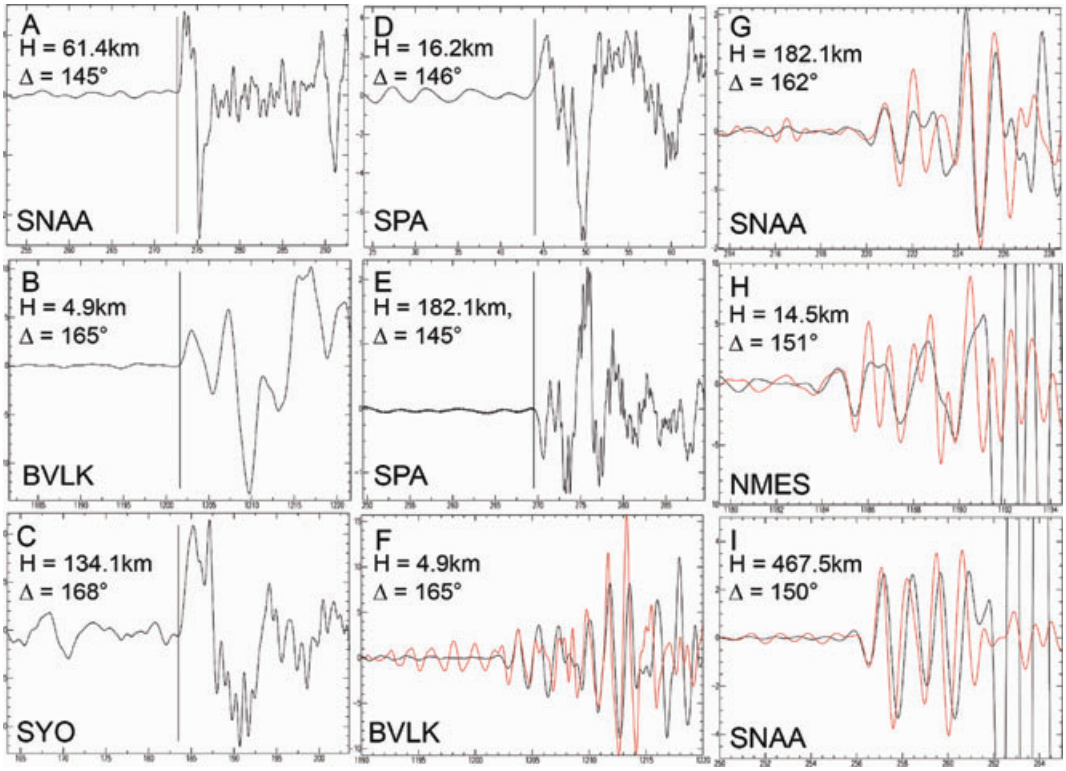

Figure 3. (a–e) Examples of PKPdf picks. (a) $M = 5.0$ event (200228714; lat. = 41.230°, lon. = 142.202); (b) $M = 8.0$ event (200230721; lat. = 63.541°, lon. = −147.731); (c) $M = 5.6$ event (200120907; lat. = 59.006°, lon. = −155.09); (d) $M = 5.2$ event (200121423; lat. = 56.225°, lon. = 163.701); (e) $M = 6.2$ event (200316722; lat. = 55.466°, lon. = 159.934); (f, g) Cross-correlation of phases after filtering. (f) PKPdf (black), PKPab(red), $M = 8.0$ event (200230721; lat. = 63.541°, lon. = −147.731); (g) PKPdf (black), PKPab (red), $M = 6.2$ event (200316722; lat. = 55.466°, lon. = 159.943°); (h) PKPdf (black), PKPbc (red), $M = 6.6$ event (200305003; lat. = 53.607°, lon. = −164.732°); (i) PKPdf (black), PKPbc (red), $M = 6.3$ event (200320806; lat. = 47.119°, lon. = 139.2520°).

3 RESULTS

Fig. 4 shows how the new data compare to previous measurements. All the new data points sample along polar paths, with the angle ξ between the PKPdf ray in the inner core and the Earth's rotation axis less than 35°. These paths are poorly covered in the previous data set, with the exception of South Atlantic events recorded at multiple Alaskan and Siberian stations. Sampling of paths with $\xi \leq 15°$ is still minimal. The mean of the new differential traveltime residuals (Figs 4a and b) along polar paths is more than 3 s smaller than many polar measurements in Tkalčić *et al*. (2002). These small polar residuals support weak anisotropy in the inner core along paths that the new data sample and reinforce findings that the South Atlantic data recorded in the northern hemisphere are considerably influenced by the structure in the mantle (Bréger *et al.* 2000; Tkalčić *et al.* 2002; Romanowicz *et al.* 2003). If there is a strong anisotropy in the inner core with fast axis aligned with the rotation axis of the Earth, then the same effect would be expected for the north–south and the south–north paths, which is not the case here. The PKPdf data in Fig. 4(c) follow the same trend as the previous data set, however the mean is shifted ≈2s closer to the zero level than previous measurements along polar paths. The most negative residuals tend to be of lower quality, corresponding to stronger attenuation of PKPdf. This confirms the correlation between earlier PKPdf arrivals and stronger attenuation, as found by Creager (1992) and Souriau & Romanowicz (1996, 1997).

Figs 5 and 6(a) show traveltime residuals with respect to the sampling of PKPdf in the inner core. For clarity, only quasi polar paths ($\xi < 35°$) are shown. New PKPdf measurements sampling the quasi-eastern hemisphere defined by Tanaka & Hamaguchi (1997) are slower than those in the quasi-western hemisphere and the observed anisotropy is weaker, but still present. In both hemispheres there are measurements down to a bottoming radius of 400 km. The sampling of the quasi-western hemisphere with differential traveltimes is poor, with only three PKPbc-df and four PKPab-df measurements recorded. This may be due to the stronger attenuation of more advanced PKPdf arrivals making it more difficult to measure differential times through cross correlation. Only two of these new residuals are larger than those found in the quasi-eastern hemisphere. This is consistent with the previous differential traveltime measurements made at Antarctica sampling the western hemisphere, which do not show a significant difference from those in the quasi-eastern hemisphere. The difference between the two hemispheres is most apparent in absolute traveltimes and the new data confirm a boundary at ≈177°E first identified by Tanaka & Hamaguchi (1997). The small differential traveltime residuals and moderate absolute traveltime residuals in the quasi-eastern hemisphere imply that PKPab and PKPbc are also slightly advanced.

Figs 6(b) and 7 show the new coverage of the lowermost mantle in comparison to previous studies from Tkalčić *et al.* (2002) and Garcia *et al*. (2006). While Tkalčić *et al.* (2002) considered only high-quality hand-picked data, Garcia *et al*. (2006) derived a large data set from automatic picks using the simulated annealing method (Chevrot 2002; Garcia *et al.* 2004). The new data recorded at GSN stations supplement the previous small number of measurements. The SSCUA stations provide coverage of a previously unsampled

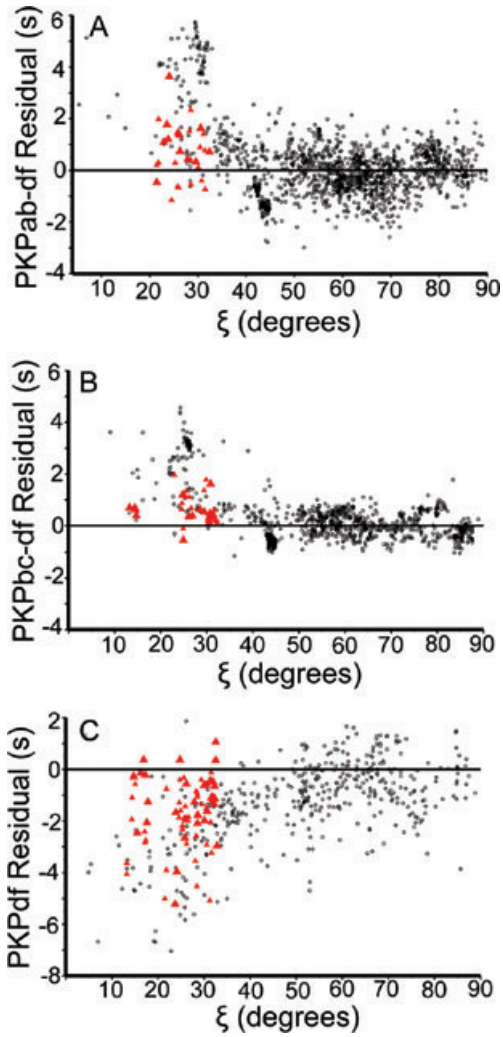

Figure 4. Traveltime residuals with respect to the model ak135 (Kennett *et al.* 1995) plotted against angle between PKPdf in the inner core and Earth's rotation axis, ξ. (a) Differential traveltime residuals PKPab-df; (b) Differential traveltime residuals PKPbc-df; (c) Absolute traveltime residuals PKPdf. New data are in red triangles. Smaller triangles indicate lower quality data. Data from Tkalčić *et al*. (2002) are plotted with open circles.

region of the CMB beneath Antarctica, at a longitude of 90°E. As a result, there is now excellent coverage of the CMB underneath Antarctica between the longitudes 60°W and 120°E. The new differential traveltimes measured in this region are not anomalous. With this improved polar sampling, existing models of the lowermost mantle may be extended to beneath the South Pole.

4 IMPLICATIONS FOR THE STRUCTURE OF THE INNER CORE

4.1 Lower mantle heterogeneity

Fig. 7 demonstrates how the new data set significantly improves the coverage of the CMB beneath Antarctica. The observed residuals are consistently less than 2 s for both PKPbc-df and PKPab-df and are significantly smaller than those observed along the SSI to Alaska path. It is difficult to attribute the size of the traveltime residuals from the SSI events to large scale structure in the inner core, as such a large anomaly is not observed along these new polar paths. Since the PKP waves observed in this study cross the CMB at multiple locations, it is unlikely that short-scale structure in the lowermost mantle is the cause of the small residuals. The new data confirm the results of the analysis of S3KS–SKKS residuals by Souriau *et al*. (2003) that no large anomalies are present at the CMB beneath the southern polar cap.

Numerous studies have argued in favour of a simple, axially symmetric model of inner core anisotropy and suggested that apparent complexity may be due to structure in the lowermost mantle (Bréger *et al.* 2000; Tkalčić *et al.* 2002; Ishii *et al.* 2002a). In Figs 8(a) and (b), events corresponding to anomalous clusters in the PKPab-df and PKPbc-df data sets are removed. These clusters correspond to well sampled paths from the South Sandwich Islands to Alaska and from Bouvet Island to California, for which sensitivity to lower mantle structure has been demonstrated in previous studies (e.g. Romanowicz *et al.* 2003). Romanowicz *et al.* (2003) found that PKPdf and PKPbc residuals from the South Atlantic events experienced the same fast transition from fast to slow, which suggested the significant part of anomaly was not caused by structure in the inner core. The new data improve the sampling of the inner core for small values of angle ξ and hence allow these anomalous paths to be identified as outliers with more certainty.

4.2 Heterogeneity within the tangent cylinder of the outer core

One hypothesis put forward is that the normal mode data may be explained by a simple inner core anisotropy model combined with heterogeneity in the outer core (Romanowicz & Bréger 2000). Romanowicz *et al.* (2003) considered a cylinder tangent to the inner core with different convective properties (Olson *et al.* 1999) in which PKP waves travel 1 per cent faster than outside to explain the body wave data of PKP traveltime residuals. The tangent cylinder model can efficiently explain the characteristic L-shaped pattern of the traveltime residuals when they are plotted as a function of the angle between PKPdf in the inner core and the rotation axis of the Earth. The data in their data set were traveltime data reported in Tkalčić *et al.* (2002) with addition of a new data set from short period stations in Alaska that recorded events from the South Atlantic Ocean. The polar paths were dominated by the southern events recorded in the northern hemisphere, and as a result the interior of the southern part of the tangent cylinder was poorly covered. With the data set reported here, we have a new opportunity to evaluate the tangent cylinder model. The boundary of the tangent cylinder parallel to the Earth's rotation axis is marked in Fig. 7. The new paths sample the cylinder in the southern hemisphere and miss it in the north. Hence, we can only constrain the properties of the southern half with the new data.

The absolute time spent within the tangent cylinder was calculated for the PKPdf waves and differential traveltime spent within the tangent cylinder was calculated for the PKPdf and PKPbc waves. In Fig. 8(c), observed PKPdf residuals from this study and Tkalčić *et al.* (2002) are plotted with respect to the time spent in the tangent cylinder. One conclusion is that the time spent within the cylinder only has a minor effect on the observed residuals. As the scatter in traveltime residuals is large, it is difficult to see a linear trend, although, in general the residuals tend to be positive for shorter times spent within the tangent cylinder and negative for longer times spent within the tangent cylinder. For PKPdf paths spending greater than 250 s within the cylinder, the majority of the observed residuals are

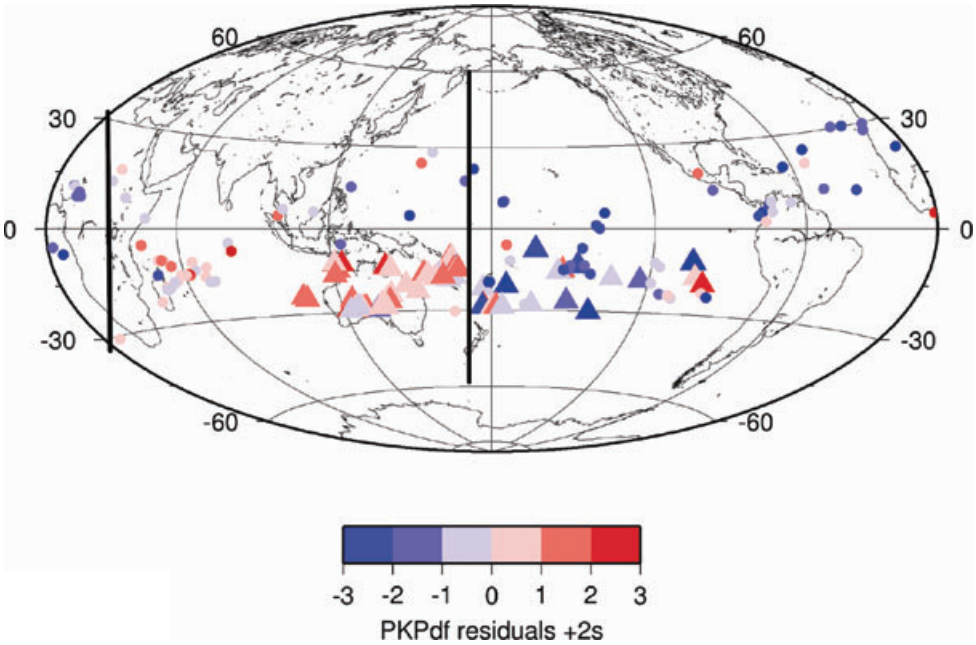

Figure 5. Bottoming points of PKPdf in the inner core for polar paths ($\xi < 35^\circ$). Colour indicates the magnitude of the observed residuals. Data from this study are shown in triangles, while data from Tkalčić *et al*. (2002) are shown in circles. The black lines mark the boundary between the quasi-eastern and western hemispheres defined by Tanaka & Hamaguchi (1997).

smaller than the values expected from the velocity anomaly of 1 per cent proposed by Romanowicz *et al.* (2003). As the largest residuals all occur along polar paths, and it is also likely that at least a part of the signal originates from structure confined within the inner core.

The differential traveltime spent within the tangent cylinder was calculated for the PKPdf and PKPbc waves. The tangent cylinder hypothesis predicts that the most anomalous differential traveltime residuals would result along paths sampling its edge, as only one phase would travel through it and therefore the largest time difference with respect to the spherically symmetric earth model would be accrued. Deeper within the cylinder, both PKPdf and PKPbc would be advanced, resulting in smaller residuals. Romanowicz *et al*. (2003) had insufficient data to test this hypothesis along polar paths from the north to the south. Fig. 8(d) shows observed residuals along polar paths with respect to the difference in the times PKPdf and PKPbc spend in the tangent cylinder. The prominent cluster of residuals to the upper right of the plot correspond to the SSI to Alaska path. As predicted, they sample the edge of the cylinder, hence PKPdf spends significantly more time within the cylinder than PKPbc, and this would result in the large residuals.

The new data recorded in Antarctica sample the inner core at a similar angle to the ray-paths from the SSI events, hence any difference in residuals should be due to the different sampling of the tangent cylinder. A velocity anomaly of 1 per cent correctly predicts the magnitude of the SSI residuals. This anomaly should appear as a positive gradient in the new observations from the north to the south between -100 and $+100$ s, but none is clearly present. We examined whether an orientation of the tangent cylinder at an angle to the Earth's rotation axis is more compatible with the observations. A tilt to the cylinder has no physical basis, but it serves to illustrate the best possible result from this class of model. Fig. 9 shows the results of a detailed grid search for the possible orientations of the cylinder, where the cylinder tilt and azimuth are free parameters in the search, incremented in steps of 5° and 20°, respectively. The model fit is determined by the correlation coefficient between the residuals and the time difference within the cylinder. If a velocity anomaly within the cylinder is the sole cause of the residuals, there should be a strong correlation. A slight tilt towards the eastern hemisphere appears to fit the data better than for a cylinder that is parallel to the rotation axis. In Fig. 8(e) the cylinder has been tilted by 9° with respect to the Earth's rotation axis, at an azimuth of 12°. Although most of the data correlate strongly with the difference in time spent within the cylinder, the SSI events remain outliers and require a larger velocity anomaly. As this orientation provides the best fit to the observations, it appears that a tangent cylinder cannot explain all of the polar residuals.

The new data indicate that there is no significant velocity anomaly within the southern half of the tangent cylinder. This is in agreement with the results of Souriau *et al*. (2003) and Yu *et al*. (2005) (body waves), and Ishii & Dziewonski (2005) (normal modes), which did not find significant heterogeneity within the tangent cylinder. Alternatively, if there is heterogeneity near the ICB confined within the tangent cylinder in the outer core, our data indicate that it is only present at the northern cap.

4.3 Cylindrical anisotropy in the inner core

The constant anisotropy model, such as one proposed by, for instance, Tromp (1995), in the case when normal modes are considered, or one proposed by Ishii *et al.* (2002a) in the case when traveltime data are binned in groups and averaged, predicts PKPbc-df residuals of 2 s and PKPab-df residuals of 4 s along polar paths. Such a model, however, overestimates the residuals observed on Antarctic stations. Our data set requires cylindrical anisotropy in the inner core to be very weak to account for the small differential traveltime residuals observed.

Quantitative estimates of the strength were obtained through a least-squares fit of observed residuals, including those from Tkalčić *et al*. (2002), to the cylindrical anisotropy parametrization from

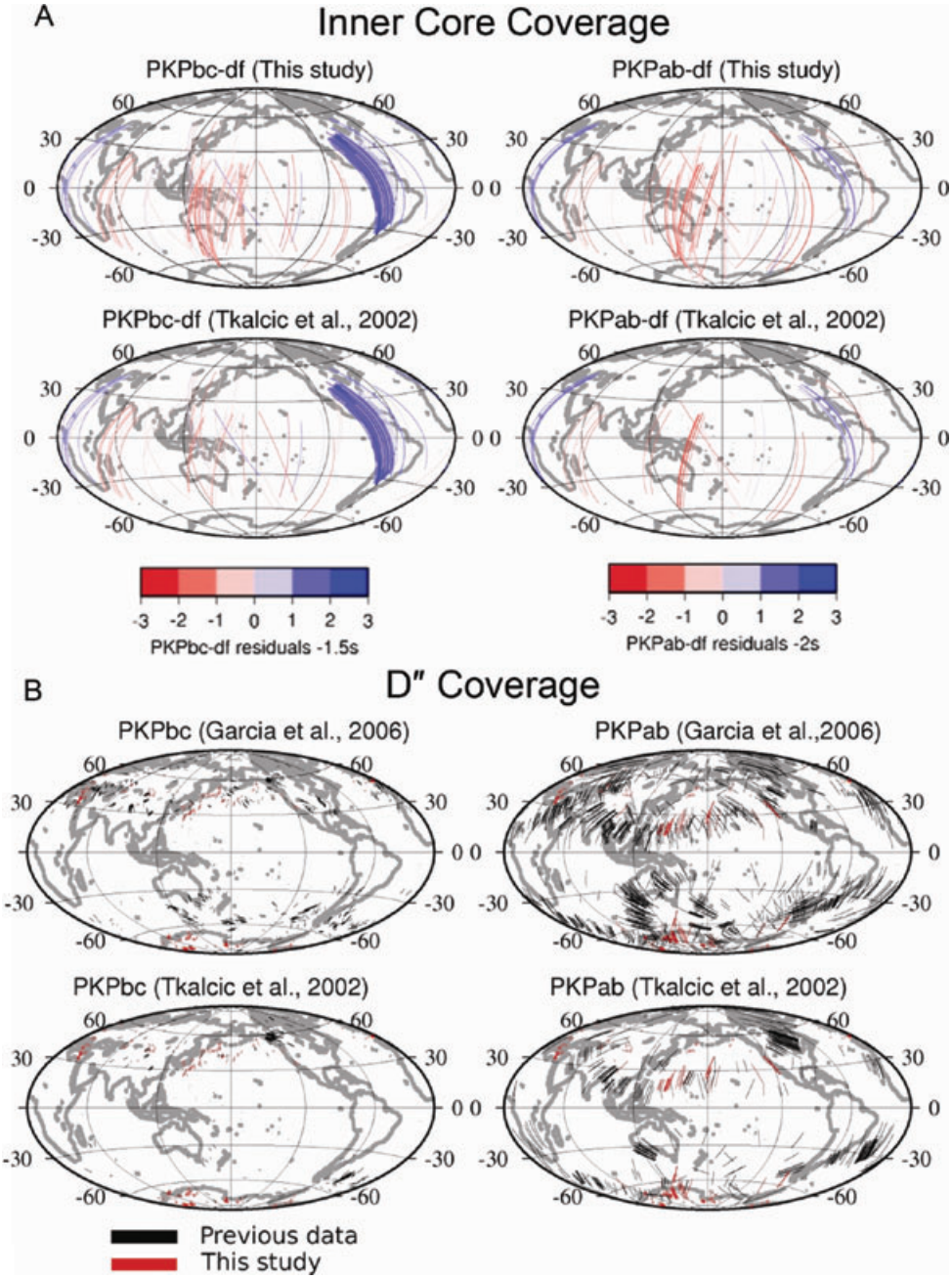

Figure 6. (a) Residuals for polar paths ($\xi < 35^\circ$) plotted with respect to the path of PKPdf through the inner core for PKPbc-df (left-hand panel) and PKPab-df (right-hand panel). The lower plots show the coverage from the data set of Tkalčić *et al*. (2002). The upper plots show the improved coverage when the new data from this study are included. The scales are offset by 1.5 s (PKPbc-df) and 2.0 s (PKPab-df) to give a contrast between the hemispheres. (b) Sampling of the deepest 300 km of the mantle along polar paths ($\xi < 35^\circ$) by PKPbc (left-hand panel) and PKPab (right-hand panel). The data sets of Garcia *et al*. (2006) (top panel) and Tkalčić *et al*. (2002) (bottom panel) are shown in comparison.

Creager (1992). Error estimates were derived from the standard errors in these parameters. The model derived from the PKPbc-df data set, after well recorded South Atlantic events are replaced by summary rays, supports an anisotropy level of (2.2 ± 0.1) per cent, with a variance reduction of 50 per cent. Polar residuals are spread ± 2 s from the model prediction in this case, in comparison to ± 1 s for equatorial residuals, and must be explained by other structure. This represents an upper bound for cylindrical anisotropy, as it cannot be increased without reducing the fit to the new observations. To estimate the level of anisotropy along the new ray paths, only the new PKPbc-df data were considered for $\xi < 35^\circ$. Data from Tkalčić *et al*. (2002) were used for $\xi > 35^\circ$ to determine the equatorial velocity. This gives a weak anisotropy of (0.7 ± 0.1) per cent.

Calvet *et al*. (2006) examined the effect of initial assumptions on inversions for cylindrical anisotropy models. As our observed residuals do not increase significantly with epicentral distance, they are most compatible with models where anisotropy decreases with depth. This corresponds to the inversions by Calvet *et al*. (2006) for smooth models with minimal constraints to their parameters. Models where the parameters are assumed to be negative, or where

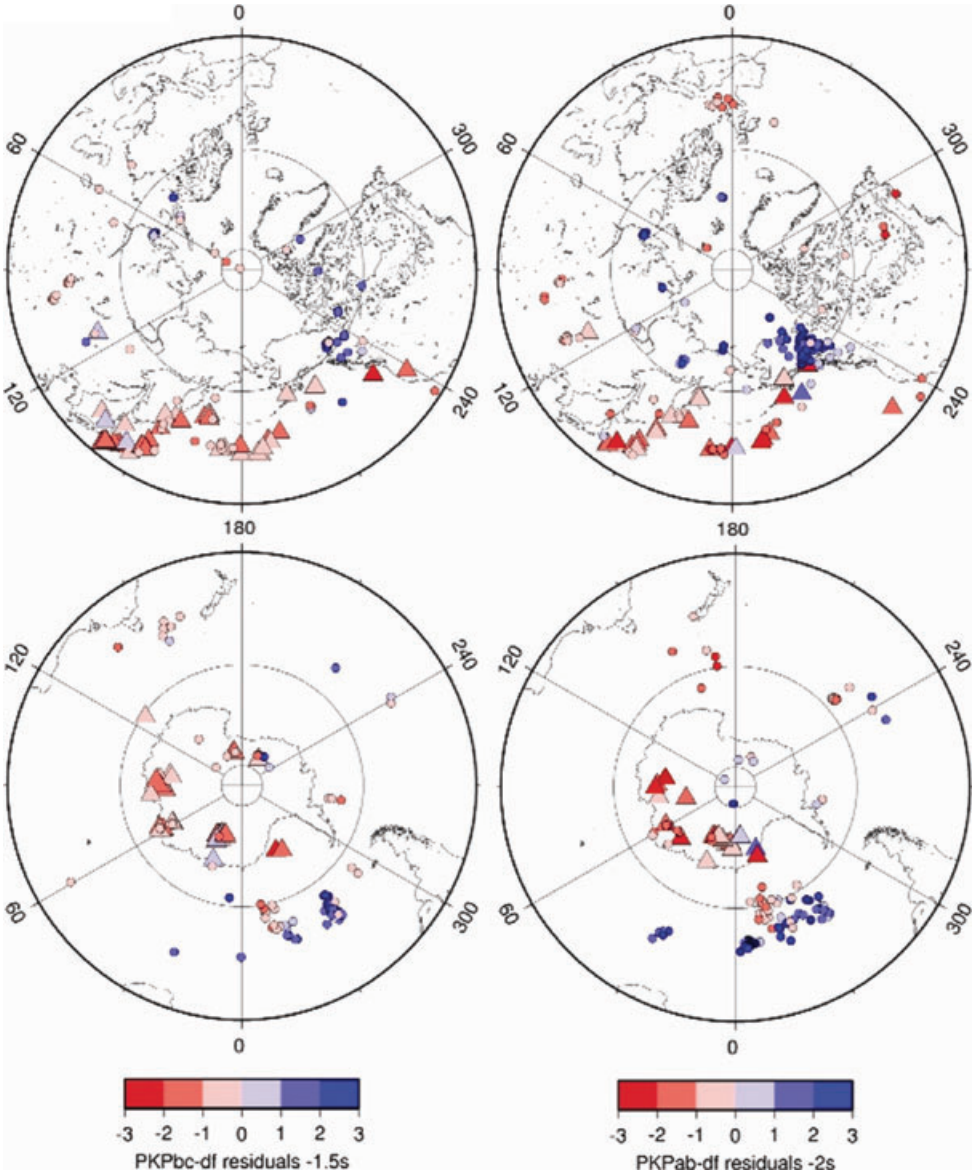

Figure 7. Residuals for polar paths ($\xi < 35^\circ$) plotted with respect to points where PKPdf crosses the core–mantle boundary. Left-hand panel: PKPbc-df residuals. Right-hand panel: PKPab-df residuals. Top: viewed from northern hemisphere. Bottom: viewed from southern hemisphere. The middle circle outlines the cylinder tangent to the inner core and parallel to the Earth's rotation axis. Data from this study are shown in triangles, while data from Tkalčić *et al*. (2002) are shown in circles.

the inner core is divided into two layers, overestimate the increase in our observed residuals with depth.

4.4 Hemispheric variation in inner core anisotropy

The new differential time residuals almost exclusively sample the quasi-eastern hemisphere of the inner core, defined by Tanaka & Hamaguchi (1997) to lie between 43°E and 177°E. A least squares fit of the new PKPbc-df residuals and those from Tkalčić *et al*. (2002) bottoming in the quasi-eastern hemisphere gives (0.4 ± 0.1) per cent cylindrical anisotropy, supporting the hypothesis that it is only weakly anisotropic. Using only new observations for $\xi < 35^\circ$ gives (0.35 ± 0.1) per cent, which is not a significant difference. Sampling of the quasi-western hemisphere is still limited and may be biased by the anomalous paths from South Atlantic mentioned previously.

The hemispheric variation was observed in the new PKPdf measurements, which sample both hemispheres. The quasi-eastern hemisphere appears to have a faster *P* velocity, resulting in small residuals. This is in agreement with observations by Tanaka & Hamaguchi (1997) along equatorial paths. Polar measurements sampling the quasi-western hemisphere result in larger residuals. These observations are consistent with the results of Tanaka & Hamaguchi (1997), Tkalčić *et al*. (2002), Niu & Wen (2002) and Garcia *et al*. (2006).

4.5 Layered inner core structure

Song & Helmberger (1998) showed that the outer portion of the inner core could be isotropic, and that anisotropy only begins 100–300 km below the inner core boundary. Residuals were separated according to the bottoming depth of PKPdf to test this hypothesis.

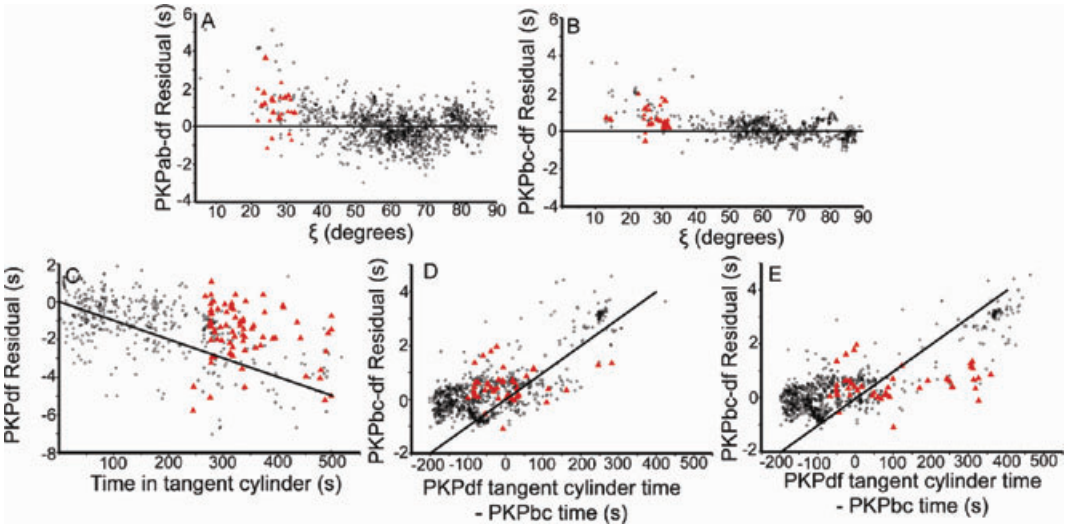

Figure 8. Differential traveltime residuals with respect to the model ak135 (Kennett *et al.* 1995). New data are shown in red triangles. (a, b) Residuals plotted against angle between PKPdf and Earth's rotation axis, ξ. The most anomalous paths in the old data mentioned in Section 4.1 have been removed. (c, d, e) Residuals plotted as a function of the traveltime spent within the tangent cylinder. Absolute PKPdf residuals are plotted in (c) and differential PKPbc-df residuals are plotted in (d) and (e). The line shows the trend expected from a 1 per cent faster velocity within the cylinder. The entire data set of Tkalčić *et al*. (2002) is plotted with open circles. In (c) and (d) the cylinder is parallel to the Earth's rotation axis, while in (e) the cylinder is tilted at an angle of 9° and azimuth of 12°.

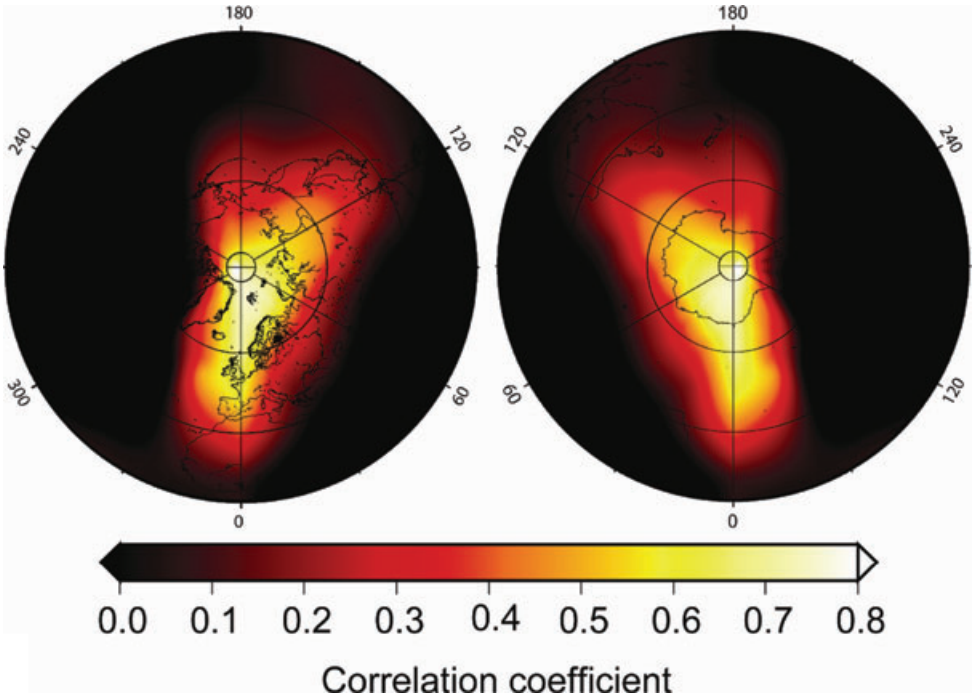

Figure 9. Fit of the tangent cylinder model to observed PKPbc-df residuals from this study and Tkalčić *et al*. (2002) with respect to its orientation. The tilt of the cylinder with respect to the Earth's rotation axis is represented by the radius. At the centre the cylinder is aligned parallel to the Earth's rotation axis. Left-hand panel: orientation viewed from northern hemisphere. Right-hand panel: orientation viewed from southern hemisphere.

The anomalous South Atlantic events discussed previously were not included in Fig. 10.

In Fig. 10, the dependence of residuals on angle ξ is slightly greater for PKPdf rays bottoming beneath the hypothesized outer isotropic layer. The transition for PKPab-df is more pronounced, however the isotropic layer is poorly sampled. Furthermore, different trends for $\xi > 40°$ visible in the PKPab-df observations in Fig. 10(c) are a result of different geographical sampling, where the near-source effects of subduction zones where most events originate, and the lowermost mantle heterogeneity effects on PKPab branch are strong. The PKPbc-df residuals from the top 200 km of the quasi-eastern hemisphere are consistent with (0.1 ± 0.2) per cent cylindrical anisotropy, using the same least squares fit as the previous sections. PKPbc-df residuals bottoming at depths greater than 200 km gave (0.6 ± 0.2) per cent cylindrical anisotropy.

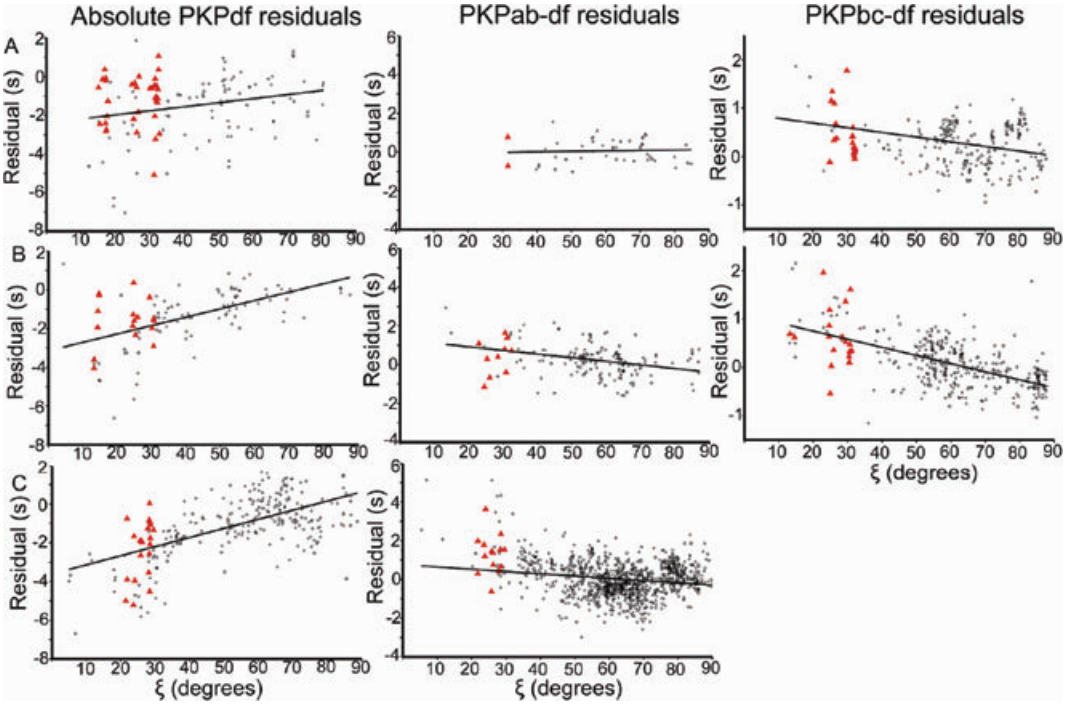

Figure 10. Residuals with respect to the model ak135 (Kennett *et al.* 1995) with lines of best fit, plotted against angle between PKPdf and Earth's rotation axis, ξ, grouped and displayed with respect to the depth of the bottoming radius of PKPdf. (a) PKPdf bottoming at a radius greater than 1000 km. (b) PKPdf bottoming at a radius between 900 and 1000 km. (c) PKPdf bottoming at a radius less than 900 km. New data are plotted in red triangles and data from Tkalčić *et al*. (2002) in circles. Smaller triangles indicate lower quality data. The anomalous paths in the old data mentioned in the Section 4.1 have been removed.

Wen & Niu (2002) examined isotropy at the top of the inner core. Our data supplement their polar observations with additional events from the north Pacific which support the isotropy in the outer 200 km of the eastern hemisphere.

Ishii & Dziewonski (2002) observed evidence for an innermost inner core with a radius of approximately 300 km in body wave data. While normal modes (Beghein & Trampert 2003) confirmed this observation, other body wave studies by Cormier & Stroujkova (2005) and Garcia *et al*. (2006) did not. Since the new observations are mainly focused on increasing constraints along the polar paths, we do not have enough new paths sampling the centremost part of the inner core to draw any conclusions about it. The largest epicentral distance observed was 174° and the majority of observations were less than 165° away, avoiding the innermost inner core.

5 FUTURE WORK

The new station QSPA is significantly more sensitive than the previous South Pole station SPA. There were 6 suitable PKPdf arrivals observed in year 2006 alone, which indicates the potential for more polar measurements in the future. Other data from high-latitudes may also result from the recent TAMSEIS and current GAMSEIS temporary broad-band seismic deployments in the Antarctic interior. The configuration of sources and the station QSPA resulted in the smallest values for angle ξ out of all the Antarctic stations, ranging from 13° to 18°. The only problem with PKP measurements at the South Pole is that the distribution of earthquakes in the northern hemisphere limited the maximum epicentral distance observed to 153°. The lack of significant seismic activity at the North Pole means that QSPA is unlikely to yield information about the deepest part of the inner core. Stations located at other locations in the interior of Antarctica would be able to probe deeper, while still observing small ξ values. For example, a station located between the South Pole and the coastal bases SANAE IV and Maitri, ideally at a latitude between 75°S and 80°S, would observe typical north Pacific events at epicentral distances of approximately 160° and angles ξ of 20°.

None of the new polar paths sample deep enough to test the innermost inner core hypothesis of Ishii & Dziewonski (2002). Antipodal observations were prevented by the lack of significant seismic activity near the North Pole combined with poor signal-to-noise ratios. Search for new core-sensitive data, such as PKPPKP waves (e.g. Tkalčić *et al.* 2006), PKJKP waves (e.g. Deuss *et al.* 2000; Cao *et al.* 2005; Wookey & Helffrich 2008), SmKS (e.g. Tanaka 2007) and PKIIKP (e.g. Niu & Chen 2008) might remain the only alternative tool to improve the sampling of both the inner and the outer core with body waves.

Models of lower mantle compressional velocity structure may benefit from new measurements crossing the CMB beneath the South Pole, as previously there were insufficient data to study this region. There is now sampling underneath most of Antarctica with PKPdf, with the Antarctic Peninsula being the main exception. Differential traveltime measurements provide valuable new polar observations and the improved coverage will assist in the identification of bias present in existing coverage of the lowermost mantle.

6 CONCLUSION

The new PKP traveltime measurements provide new data along previously poorly sampled polar paths and provide excellent coverage of the CMB beneath half of Antarctica. Sampling of the inner core along polar paths is significantly improved and provides closer constraints for current models. An axially symmetric model of inner core anisotropy derived from PKPbc-df observations requires

only weak (0.7 ± 0.1) per cent anisotropy. . Coverage of the quasi-western hemisphere along polar paths with differential traveltimes still needs improvement and may be biased by measurements along the South Atlantic to Alaska path, as the new differential time residuals from this study are consistently smaller than 2 s. Furthermore, there is no evidence of a velocity anomaly near the ICB in the southern cap of the cylinder tangent in the outer core, but we cannot disprove the existence of such an anomaly on the northern cap. The new data are not inconsistent with the hypothesis of hemispherical variation of inner core anisotropy beneath an isotropic outer layer with (0.1 ± 0.2) per cent anisotropy observed in the top 200 km of the quasi-eastern hemisphere compared to an average over all depths sampled by PKPbc-df of (0.4 ± 0.1) per cent.

ACKNOWLEDGMENTS

Field logistic support of the temporary SSCUA stations was provided by the Australian Antarctic Division. The facilities of the IRIS Data Management System, and specifically the IRIS Data Management Center, were used for access to waveform and metadata required in this study. The IRIS DMS is funded through the National Science Foundation and specifically the GEO Directorate through the Instrumentation and Facilities Program of the National Science Foundation under Cooperative Agreement EAR-0552316. IRIS provided data from the permanent Antarctic stations SNAA, QSPA, SPA, SYO, MAW and VNDA. We thank two anonymous reviewers and Mike Kendall for their constructive comments.

REFERENCES

Beghein, C. & Trampert, J., 2003. Robust normal mode constraints on inner core anisotropy from model space search, *Science,* **299,** 552–555.

Bergman, M.I., 1997. Measurements of elastic anisotropy due to solidification texturing and the implications for the Earth's inner core, *Nature,* **389,** 60–63.

Bergman, M.I., Haskel, M., Chandler, B. & Akpan, N., 2005. A laboratory model for solidification of Earth's core, *Phys. Earth planet. Inter.,* **153,** 150–164.

Bréger, L., Romanowicz, B. & Tkalčić, H., 1999. PKP(BC-DF) travel time residuals and short scale heterogeneity in the deep Earth, *Geophys. Res. Lett.,* **20,** 169–172.

Bréger, L., Tkalčić, H. & Romanowicz, B., 2000. The effect of D" on PKP(AB-DF) travel time residuals and possible implications for inner core structure, *Earth planet. Sci. Lett.,* **175,** 133–143.

Buffet, B.A. & Wenk, H.R., 2001. Texturing of the Earth's inner core by Maxwell stresses, *Nature,* **413,** 60–63.

Calvet, M., Chevrot, S. & Souriau, A., 2006. P-wave propagation in transversely isotropic media II. Application to inner core anisotropy: Effects of data averaging, parameterizarion and a priori information, *Phys. Earth planet. Inter.,* **156,** 21–40.

Cao, A., Romanowicz, B. & Takeuchi, N., 2005. An observation of PKJKP: inferences on inner core shear properties, *Science,* **308,** 1453–1455.

Chevrot, S., 2002. Optimal measurement of relative and absolute delay times by simulated annealing, *Geophys. J. Int.,* **151,** 164–171.

Cormier, V.F. & Stroujkova, A., 2005. Waveform search for the innermost inner core, *Earth planet. Sci. Lett.,* **236,** 96–105, doi:10.1016/j.epsl.2005.05.016.

Creager, K.C., 1992. Anisotropy of the inner core from differential travel times of the phases PKP and PKIKP, *Nature,* **356,** 309–314.

Creager, K.C., 1999. Large-scale variations in inner-core anisotropy, *J. geophys. Res.,* **104,** 23 127–23 139.

Deuss, A., Woodhouse, J.H., Paulssen, H. & Trampert, J., 2000. The observation of inner core shear waves, *Geophys. J. Int.,* **142,** 67–73.

Doornbos, D.J., 1974. Seismic wave scattering near caustics: observation of PKKP precursors, *Nature,* **247,** 34–35.

Dziewonski, A.M. & Anderson, D.L., 1981. Preliminary reference Earth model, *Phys. Earth planet. Inter.,* **25,** 297–356.

Engdahl, E.R., van der Hilst, R.D. & Buland, R.P., 1998. Global teleseismic earthquake relocation with improved travel times and procedures for depth determination, *Bull. seism. Soc. Am.,* **88,** 722–743.

Garcia, R., 2001. Constraints on upper inner core structure by waveform inversion of core phases, *Geophys. J. Int.,* **150,** 651–664.

Garcia, R., Chevrot, S. & Weber, M., 2004. Non linear waveform and delay time analysis of triplicated core phases, *J. geophys. Res.,* **109,** B01306, doi:10.1029/2003JB002429.

Garcia, R., Tkalčić, H. & Chevrot, S., 2006. A new global PKP data set to study Earth's core and deep mantle, *Phys. Earth planet. Inter.,* **159,** 15–31.

Garnero, E.J. & Helmberger, D.V., 1995. A very slow basal layer underlying large-scale low velocity anomalies in the lower mantle beneath the Pacific: evidence from core phases, *Phys. Earth planet. Inter.,* **91,** 161–176.

Haddon, R.A.W. & Cleary, J.R., 1974. Evidence for scattering of seismic PKP waves near the mantle–core boundary, *Phys. Earth planet. Inter.,* **8,** 211–234.

Helffrich, G. & Sacks, S., 1994. Scatter and bias in differential PKP travel times and implications for mantle and core phenomena, *Geophys. Res. Lett.,* **21,** 2167–2170.

Helffrich, G., Kaneshima, S. & Kendall, J.-M., 2002. A local, crossing-path study of attenuation and anisotropy of the inner core, *Geophys. Res. Lett.,* **29**(12), 1568, doi:10.1029/2001GL014059.

Ishii, M. & Dziewonski, A.M., 2002. The innermost inner core of the earth: evidence for a change in anisotropic behavior at a radius of about 300 km, *Proc. Natl. Acad. Sci. U.S.A.,* **99,** 14 026–14 030.

Ishii, M. & Dziewonski, A.M., 2005. Constraints on the outer-core tangent cylinder using norml-mode splitting measurements, *Geophys. J. Int.,* **162,** 787–792.

Ishii, M., Tromp, J., Dziewonski, A.M. & Ekstrom, G., 2002a. Joint inversion of normal mode and body wave data for inner core anisotropy, 1: laterally homogeneous anisotropy, *J. geophys. Res.,* **107**(B12), 2379, doi:10.1029/2001JB000712.

Ishii, M., Tromp, J., Dziewonski, A.M. & Ekstrom, G., 2002b. Joint inversion of normal mode and body wave data for inner core anisotropy, 2; possible complexities, *J. geophys. Res.,* **107**(B12), 2380, doi:10.1029/2001JB000713.

Jeanloz, R. & Wenk, H.R., 1988. Convection and anisotropy of the inner core, *Geophys. Res. Lett.,* **15,** 72–75.

Karato, S.-I., 1993. Inner core anisotropy due to the magnetic field-induced preferred orientation of iron, *Science,* **262,** 1708–1711.

Karato, S.-I., 1999. Seismic anisotropy of the Earth's inner core resulting from flow induced by Maxwell stresses, *Nature,* **402,** 871–873.

Kennett, B.L.N., Engdahl, E.R. & Buland, R., 1995. Constraints on seismic velocities in the Earth from traveltimes, *Geophys. J. Int.,* **122,** 108–124.

Morelli, A., Dziewonski, A. & Woodhouse, J., 1986. Anisotropy of the inner core inferred from PKIKP travel times, *Geophys. Res. Lett.,* **13,** 1545–1548.

Niu, F. & Chen, Q.-F., 2008. Seismic evidence for distinct anisotropy in the innermost inner core, *Nat. Geosci.,* **1,** 692–696.

Niu, F. & Wen, L., 2002. Seismic anisotropy in the top 400 km of the inner core beneath the "eastern" hemisphere, *Geophys. Res. Lett.,* **29,** 1611, doi:10.1029/2001GL014118.

Olson, P., Christensen, U. & Glatzmaier, G.A., 1999. Numerical modeling of the geodynamo: Mechanisms of field generation and equilibration, *J. geophys. Res.,* **104**(B5), 10 383–10 404.

Ouzounis, A. & Creager, K.C., 2001. Isotropy overlying anisotropy at the top of the inner core, *Geophys. Res. Lett.,* **28,** 4331–4334.

Poupinet, G., Pillet, R. & Souriau, A., 1983. Possible heterogeneity in the Earth's core deduced from PKIKP travel times, *Nature,* **305,** 204–206.

Reading, A.M., 2006. The seismic structure of Precambrian and early Palaeozoic terranes in the Lambert Glacier region, East Antarctica, *Earth planet. Sci. Lett.,* **244,** 44–57.

Restivo, A. & Helffrich, G., 2006. Core-mantle boundary structure investigated using SKS and SKKS polarization anomalies, *Geophys. J. Int.,* **165,** 288–302, doi:10.1111/j.1365-246X.2006.02901, 2006.

Romanowicz, B. & Bréger, L., 2000. Anomalous splitting of free oscillations: a reevaluation of possible interpretations, *J. geophys. Res.,* **105,** 21 559–21 578.

Romanowicz, B., Tkalčić, H. & Bréger, L., 2003. On the origin of complexity in PKP travel time data, in *Earth's Core: Dynamics, Structure, Rotation,* Vol. 31, pp. 31–44, eds Dehant, V., Creager, K.C., Zatman, S. & Karato, S-I., American Geophysical Union Geodynamics Series.

Snoke, J.A. & Sacks, I.S., 1986. Seismic modeling of lateral heterogeneity at the base of the mantle, *Geophys. J. R. astr. Soc.,* **86,** 801–814.

Song, X. & Helmberger, D.V., 1998. Seismic evidence for an inner core transition zone, *Science,* **282,** 924–926.

Souriau, A. & Poupinet, G., 1994. Lateral variations in P velocity and attenuation in the D layer, from diffracted P waves, *Phys. Earth planet. Inter.,* **84,** 227–234.

Souriau, A. & Romanowicz, B., 1996. Anisotropy in inner core attenuation: a new type of data to constrain the nature of the solid core, *Geophys. Res. Lett.,* **23,** 1–4.

Souriau, A. & Romanowicz, B., 1997. Anisotropy in the inner core attenuation: relation between P-velocity and attenuation, *Phys. Earth planet. Inter.,* **101,** 33–47.

Souriau, A., Teste, A. & Chevrot, S., 2003. Is there any structure inside the liquid outer core?, *Geophys. Res. Lett.,* **30**(11), 1567.

Stixrude, L. & Cohen, R.E., 1995. High-pressure elasticity of iron and anisotropy in the Earth's core, *Phys. Earth planet. Inter.,* **22,** 221–225.

Sylvander, M., Ponce, B. & Souriau, A., 1997. Seismic velocities at the core–mantle boundary inferred from P waves diffracted around the core, *Phys. Earth planet. Inter.,* **101,** 189–202.

Tanaka, S., 2007. Possibility of a low *P*-wave velocity layer in the outermost core from global SmKS waveforms, *Earth planet. Sci. Lett.,* **259,** 486–499.

Tanaka, S. & Hamaguchi, H., 1997. Degree one heterogeneity and hemispherical variation of anisotropy in the inner core from PKP(BC)-PKP(DF) times, *J. geophys. Res.,* **102,** 2925–2938.

Thomas, C., Kendall, J.M. & Weber, M., 2002. The lowermost mantle beneath northern Asia–I. Multi-azimuth studies of a D" heterogeneity, *Geophys. J. Int.,* **151,** 279–295.

Tkalčić, H., Flanagan, M. & Cormier, V.F., 2006. Observations of near-podal P'P' precursors: Evidence for back scattering from the 150–220 km zone in Earth's upper mantle, *Geophys. Res. Lett.,* **33,** L03305, doi:10.1029/2005GL024626.

Tkalčić, H. & Kennett, B.L.N., 2008. Core structure and heterogeneity: a seismological perspective, *Aust. J. Earth Sci.,* **55,** 419–431.

Tkalčić, H., Romanowicz, B. & Houy, N., 2002. Constraints on D" structure using PKP(AB-DF), PKP(BC-DF) and PcP-P traveltime data from broadband records, *Geophys. J. Int.,* **148,** 599–616.

Tromp, J., 1995. Normal mode splitting due to inner core anisotropy, *Geophys. J. Int.,* **121,** 963–968.

Wen, L. & Niu, F., 2002. Seismic velocity and attenuation structures in the top of the Earth's inner-core, *J. geophys. Res.,* **107,** 2273, doi:10.1029/2001JB000170.

Woodhouse, J.H., Giardini, D. & Li, X.D., 1986. Evidence for inner core anisotropy from free oscillations, *Geophys. Res. Lett.,* **13,** 321–370.

Wookey, J. & Helffrich, G., 2008. Inner-core shear-wave anisotropy and texture from an observation of PKJKP waves, *Nature,* **454,** 873–877.

Wysession, M.E., Okal, E.A. & Bina, C.R., 1992. The structure of the core mantle boundary from diffracted waves, *J. geophys. Res.,* **97,** 8749–8764.

Yoshida, S., Sumita, I. & Kumazawa, M., 1996. Growth model of the inner core coupled with the outer core dynamics and the resulting elastic anisotropy, *J. geophys. Res.,* **101,** 28 085–28 193.

Yu, W., Wen, L. & Niu, F., 2005. Seismic velocity structure in the Earth's outer core, *J. geophys. Res.,* **110,** B02302, doi:10.1029/2003JB002928.

APPENDIX

Table A1. PKPdf absolute traveltime measurements made in this study.

Time (YDH)	Lat. (°)	Lon. (°)	Depth (km)	Station code	Observed (s)	Predicted (s)	Residual (s)	Quality
200101016	59.94	−153.54	33	SPA	1181.1	1181.7	−0.6	B
200114500	44.27	148.34	33	SNAA	1180.4	1180.8	−0.4	A
200116520	51.16	−179.87	18	SYO	1189.5	1190.6	−1.1	B
200120907	59.01	−155.1	134.1	SPA	1165.2	1167.7	−2.5	A
200120907	59.01	−155.1	134.1	SYO	1187.7	1190.4	−2.7	A
200120907	59.01	−155.1	134.1	SNAA	1182.3	1186.3	−4.0	A
200121500	56.23	163.7	16.2	SPA	1178.6	1178.2	0.4	A
200121500	56.23	163.7	16.2	SYO	1188.8	1188.4	0.4	A
200217917	43.76	130.69	566	SNAA	1111.3	1111.9	−0.6	A
200220612	43.79	147.52	33	SNAA	1179.7	1179.8	−0.1	B
200225808	44.68	130.06	586.3	SNAA	1110.4	1111.0	−0.6	A
200228714	41.23	142.2	61.4	SNAA	1171.2	1170.1	1.1	A
200228910	51.92	157.22	102.4	SYO	1167.4	1168.0	−0.6	A
200228910	51.92	157.22	102.4	SNAA	1183.7	1185.0	−1.3	A
200229611	63.53	−148.16	4.2	BVLK	1204.0	1204.8	−0.8	B
200229611	63.53	−148.16	4.2	VNDA	1171.1	1176.9	−5.8	A
200229611	63.53	−148.16	4.2	SPA	1188.2	1191.8	−3.6	B
200229611	63.53	−148.16	4.2	SNAA	1200.1	1205.1	−5.0	B
200230722	63.54	−147.73	19	BVLK	1200.9	1202.4	−1.5	A
200230722	63.54	−147.73	4.9	VNDA	1172.4	1176.9	−4.5	B
200230722	63.54	−147.73	4.9	SPA	1187.7	1191.8	−4.1	B
200230722	63.54	−147.73	4.9	SNAA	1197.0	1204.9	−7.9	B
200230722	63.54	−147.73	4.9	SYO	1205.4	1210.6	−5.2	A
200231115	51.16	179.36	33	SNAA	1193.9	1195.0	−1.1	B
200232105	47.96	146.4	470.2	SNAA	1134.1	1134.5	−0.4	B

Table A1. (*Continued.*)

Time (YDH)	Lat. (°)	Lon. (°)	Depth (km)	Station code	Observed (s)	Predicted (s)	Residual (s)	Quality
200233000	51.6	−173.64	20.6	BVLK	1178.1	1178.4	−0.3	B
200233001	51.6	−173.64	20.6	SNAA	1194.3	1196.9	−2.6	B
200233101	54.66	−160.76	33	CRES	1187.2	1189.1	−1.9	B
200233101	54.66	−160.76	33	BVLK	1184.9	1187.2	−2.3	B
200236209	51.44	−168.57	10	CRES	1183.2	1185.0	−1.8	B
200236209	51.44	−168.57	10	NMES	1179.8	1182.0	−2.2	B
200236209	51.44	−168.57	10	BVLK	1179.9	1182.8	−2.9	B
200301605	44.11	−129.2	34	NMES	1176.7	1181.8	−5.1	B
200302607	52.28	−170.27	35.1	NMES	1178.0	1178.4	−0.4	B
200305003	53.61	−164.73	14.5	JACK	1186.8	1188.2	−1.4	B
200305003	53.61	−164.73	14.5	NMES	1184.2	1186.1	−1.9	B
200316619	51.57	176.86	34.2	MAW	1173.8	1173.5	0.3	B
200316619	51.57	176.86	34.2	SNAA	1195.3	1195.3	0.0	B
200316722	55.47	159.93	182.1	SPA	1155.7	1155.9	−0.2	A
200316722	55.47	159.93	182.1	SYO	1166.9	1164.5	2.4	A
200316722	55.47	159.93	182.1	SNAA	1177.5	1179.5	−2.0	A
200317412	51.47	176.74	0.7	SNAA	1196.2	1200.7	−4.5	B
200326820	41.86	143.88	27	SNAA	1175.2	1176.3	−1.1	A
200326906	42.22	144.63	28.5	SNAA	1175.6	1176.9	−1.3	A
200327221	41.48	144.1	33	SNAA	1175.2	1174.8	0.4	A
200328109	42.65	144.53	32	SNAA	1176.5	1177.0	−0.5	A
200328400	41.98	144.33	28	SNAA	1175.8	1176.5	−0.7	A
200332106	51.13	178.65	27.1	SNAA	1194.1	1195.9	−1.8	A
200332106	51.13	178.65	27.1	MAW	1174.2	1175.2	−1.0	A
200333921	55.57	165.74	9.9	SPA	1175.4	1178.2	−2.8	B
200335609	42.35	144.55	28	SNAA	1175.9	1177.2	−1.3	B
200410502	55.24	162.32	51.3	QSPA	1168.7	1171.4	−2.7	B
200416215	55.7	160.02	186.6	QSPA	1153.2	1155.6	−2.4	B
200416215	55.7	160.02	188.6	SYO	1162.7	1164.0	−1.3	B
200416215	55.7	160.02	188.6	SNAA	1177.1	1179.0	−1.9	A
200418010	54.79	−134.6	20	QSPA	1172.9	1175.0	−2.1	A
200418010	54.79	−134.6	20	SNAA	1187.8	1189.4	−1.6	B
200420108	49.52	−127.1	23.7	SNAA	1178.0	1178.0	0.0	A
200422009	51.66	−166.27	8	SNAA	1194.6	1198.1	−3.5	B
200422009	51.66	−166.27	8	MAW	1186.9	1188.4	−1.5	A
200425703	44.02	151.43	8	SNAA	1182.3	1185.5	−3.2	B
200430914	43.66	146.82	61.8	SNAA	1174.6	1175.7	−1.1	A
200431610	42.17	144.36	32.8	SNAA	1175.0	1176.1	−1.1	A
200433318	43	145.13	39	SNAA	1175.7	1176.8	−1.1	A
200434114	42.89	145.23	35	SNAA	1176.0	1177.2	−1.2	A
200505712	40.72	142.37	68	SNAA	1165.5	1168.5	−3.0	A
200516517	51.21	179.46	55.2	SNAA	1191.3	1192.2	−0.9	B
200526402	43.9	146.18	105.1	SNAA	1168.5	1170.5	−2.0	B
200531419	57.45	120.59	6	QSPA	1181.8	1181.9	−0.1	A
200611104	60.53	165.82	9	QSPA	1186.2	1186.4	−0.2	B
200611111	61.35	167.53	12	QSPA	1185.3	1187.2	−1.9	B
200611207	61.2	167.32	12	QSPA	1185.8	1186.9	−1.1	B
200611917	60.49	167.52	11	QSPA	1185.7	1186.0	−0.3	A
200611917	60.49	167.52	11	SNAA	1204.9	1206.6	−1.7	A
200614213	54.27	158.45	197	QSPA	1150.6	1151.9	−1.3	A
200618920	51.21	−179.31	22	SNAA	1194.6	1196.7	−2.1	A
200622911	55.62	161.69	55	QSPA	1171.5	1171.6	−0.1	A
200623622	51.15	157.52	43	SNAA	1190.7	1191.5	−0.8	B
200627318	46.35	153.17	11	SNAA	1187.4	1188.9	−1.5	B
200631621	48.28	154.25	36	SNAA	1186.5	1187.9	−1.4	B
200631921	47.28	154.15	12	SNAA	1188.3	1190.3	−2.0	A
200632006	46.34	154.51	9	SNAA	1186.7	1189.6	−2.9	B
200634119	46.15	154.39	16	SNAA	1186.5	1188.1	−1.6	A

Note: Residuals are with respect to the model ak135 (Kennett *et al.* 1995) and were corrected for ellipticity.

Table A2. PKPbc-df differential traveltime measurements made in this study.

Time (YDH)	Lat. (°)	Lon. (°)	Depth (km)	Station code	Observed (s)	Predicted (s)	Residual (s)	Quality
200114500	44.27	148.34	33	SNAA	4.3	4.7	0.4	A
200116520	51.16	−179.87	18	SYO	8.2	8.8	0.6	B
200121500	56.23	163.7	16.2	SYO	6.9	8.1	1.2	A
200128118	52.68	160.13	48.5	SYO	3.6	3.9	0.3	A
200229611	63.53	−148.16	4.2	SPA	7.6	6.5	−1.1	B
200230722	63.54	−147.73	4.9	CASY	3.8	5.1	1.3	B
200230722	63.54	−147.73	4.9	SPA	7.6	8.3	0.7	A
200231115	51.16	179.36	33	SYO	8.0	8.6	0.6	A
200232105	47.96	146.4	470.2	SNAA	7.2	8.6	1.4	B
200233000	51.6	−173.64	20.6	BVLK	1.7	3.0	1.3	B
200233101	54.66	−160.76	33	CRES	8.6	8.7	0.1	B
200236209	51.44	−168.57	10	CRES	4.5	5.2	0.7	B
200236209	51.44	−168.57	10	NMES	2.9	4.0	1.1	B
200236209	51.44	−168.57	10	BVLK	3.3	4.4	1.1	B
200305003	53.61	−164.73	14.5	JACK	6.6	7.0	0.4	B
200305003	53.61	−164.73	14.5	NMES	5.6	6.2	0.6	B
200320806	47.12	139.25	467.5	SNAA	5.3	5.8	0.5	A
200326920	42.06	144.52	12.2	SNAA	1.2	1.3	0.1	B
200327023	44.77	150.31	45.7	SNAA	5.1	5.4	0.3	B
200327214	42.12	144.34	35.7	SNAA	1.2	1.3	0.1	B
200328109	42.65	144.53	32	SNAA	1.9	1.9	0.0	B
200328400	41.98	144.33	28	SNAA	1.0	1.2	0.2	B
200330122	43.91	147.73	74.8	SNAA	3.9	4.2	0.3	B
200332106	51.13	178.65	27.1	SYO	7.8	8.4	0.6	B
200333921	55.57	165.74	9.9	SYO	7.1	7.1	0.0	B
200335609	42.35	144.55	28	SNAA	1.5	1.5	0.0	B
200416215	55.7	160.02	188.6	SYO	5.7	6.6	0.9	B
200418010	54.79	−134.6	20	SNAA	7.7	7.2	−0.5	A
200420108	49.52	−127.1	23.7	SNAA	1.7	2.1	0.4	A
200422009	51.66	−166.27	8	MAW	6.2	6.9	0.7	A
200425703	44.02	151.43	8	SNAA	4.6	5.2	0.6	B
200430914	43.66	146.82	61.8	SNAA	3.5	3.9	0.4	B
200433318	43	145.13	39	SNAA	2.4	2.5	0.1	B
200436321	53.16	−173.74	252.7	BVLK	3.4	3.3	−0.1	B
200501814	42.95	144.88	42	SNAA	2.3	2.5	0.2	B
200531419	57.45	120.59	8.4	SNAA	7.4	9.4	2.0	B
200611023	60.87	167.01	10	QSPA	5.5	6.1	0.6	A
200611104	60.53	165.82	9	QSPA	5.2	5.6	0.4	A
200611111	61.35	167.53	12	QSPA	5.9	6.6	0.7	B
200611207	61.2	167.32	12	QSPA	5.8	6.5	0.7	A
200611917	60.49	167.52	11	QSPA	5.2	5.6	0.4	B
200617311	45.44	149.39	95	SNAA	5.5	7.1	1.6	A
200622915	46.54	141.91	14	SNAA	4.8	6.6	1.8	B
200627318	46.35	153.17	11	SNAA	6.7	6.8	0.1	A
200627409	46.47	153.26	19	SNAA	6.8	6.9	0.1	A
200631621	48.28	154.25	36	SNAA	8.2	8.3	0.1	A
200631911	46.56	153.35	10	SNAA	6.9	7.1	0.2	A
200632006	46.34	154.51	9	SNAA	6.9	7.2	0.3	A
200634119	46.15	154.39	16	SNAA	6.7	7.2	0.5	A

Note: Residuals are with respect to the model ak135 (Kennett *et al.* 1995) and were corrected for ellipticity.

Table A3. PKPab-df differential traveltime measurements made in this study.

Time (YDH)	Lat. (°)	Lon. (°)	Depth (km)	Station code	Observed (s)	Predicted (s)	Residual (s)	Quality
200120907	59.01	−155.1	134.1	SYO	68.4	69.0	−0.6	B
200120907	59.01	−155.1	134.1	SNAA	54.5	50.9	3.6	A
200121500	56.23	163.7	16.2	SNAA	53.0	51.5	1.5	B
200220612	43.79	147.52	33	SNAA	6.6	7.3	−0.7	B
200228910	51.92	157.22	102.4	SNAA	35.3	34.9	0.4	A
200229611	63.53	−148.16	4.2	BVLK	55.0	54.7	0.3	B
200229611	63.53	−148.16	4.2	SNAA	56.1	55.9	0.2	B
200230722	63.54	−147.73	4.9	BVLK	57.2	55.2	2.0	B
200230722	63.54	−147.73	4.9	SNAA	55.0	55.5	−0.5	A
200305003	53.61	−164.73	14.5	NMES	11.6	12.8	−1.2	B
200316722	55.47	159.93	182.1	SNAA	49.4	48.0	1.4	A
200327023	44.77	150.31	45.7	SNAA	12.6	11.2	1.4	B
200330122	43.91	147.73	74.8	SNAA	8.7	7.9	0.8	B
200332106	51.13	178.65	27.1	SYO	21.0	20.6	0.4	B
200333921	55.57	165.74	9.9	SNAA	51.0	50.3	0.7	A
200516517	51.21	179.46	55.2	SNAA	37.7	38.3	−0.6	B
200531419	57.45	120.59	8.4	SNAA	20.4	19.3	1.1	A
200611023	60.95	167.09	22	SNAA	71.6	69.8	1.8	A
200611917	60.49	167.52	11	SNAA	69.5	68.3	1.2	A
200617311	45.44	149.39	95	SNAA	12.2	12.6	−0.4	B
200618920	51.21	−179.31	22	SNAA	40.3	38.0	2.3	B
200623622	51.15	157.52	43	SNAA	33.9	32.4	1.5	B
200627409	46.47	153.26	19	SNAA	17.8	16.9	0.9	B
200631621	48.28	154.25	36	SNAA	22.7	22.4	0.3	A
200631921	47.28	154.15	12	SNAA	19.6	19.5	0.1	B
200632006	46.34	154.51	9	SNAA	18.8	17.2	1.6	A

Note: Residuals are with respect to the model ak135 (Kennett *et al.* 1995) and were corrected for ellipticity.